Computer modeling of angular emission from Ag(100) and Mo(100) surfaces due to Arn cluster bombardment

Dawid Maciazek, Michal Kanski, Lukasz Gaza, Barbara J. Garrison, and Zbigniew Postawa

---

Articles you may be interested in

Sputtering yields of Ru, Mo, and Si under low energy Ar + bombardment
J. Appl. Phys. **106**, 054902 (2009); 10.1063/1.3149777

Enhancement of ultraviolet lasing from Ag-coated highly disordered ZnO films by surface-plasmon resonance
Appl. Phys. Lett. **90**, 231106 (2007); 10.1063/1.2746940

Morphology evolution on diamond surfaces during ion sputtering
J. Vac. Sci. Technol. A **23**, 1579 (2005); 10.1116/1.2110386

Real-time x-ray studies of Mo-seeded Si nanodot formation during ion bombardment
Appl. Phys. Lett. **87**, 163104 (2005); 10.1063/1.2099521

Defects and morphological changes in nanothin Cu films on polycrystalline Mo analyzed by thermal helium desorption spectrometry
J. Appl. Phys. **98**, 024315 (2005); 10.1063/1.1925765

Computer modeling of angular emission from Ag(100) and Mo(100) surfaces due to Ar_n cluster bombardment

Dawid Maciazek, Michal Kanski, and Lukasz Gaza
Smoluchowski Institute of Physics, Jagiellonian University, ul. Prof. Lojasiewicza 11, 30-348 Krakow, Poland

Barbara J. Garrison
Department of Chemistry, Penn State University, 104 Chemistry Bldg, University Park, Pennsylvania 16802

Zbigniew Postawa[a)]
Smoluchowski Institute of Physics, Jagiellonian University, ul. Prof. Lojasiewicza 11, 30-348 Krakow, Poland

Molecular dynamics computer simulations are employed to investigate the effect of projectile size and surface morphology on the angular emission stimulated by impact of Ar gas cluster projectiles. Argon clusters of sizes n = 10–1000 and kinetic energies of 10 and 20 keV Ar_n aimed at normal incidence are used to sputter Ag(100) and Mo(100) samples. The total sputtering yield is larger for Ag(100) than for Mo(100). The ratio of sputtering yields is inversely proportional to the ratio of sublimation energies of these solids for projectiles between Ar_{20} and Ar_{250}. In both systems, the angular distributions are sensitive to both the projectile size and the surface roughness. The maximum of angular spectra shifts from direction normal to the surface toward off-normal direction with the increase in the projectile size. An opposite trend is observed with the increase in the surface roughness. Formation of a cloud composed of projectile atoms and the enhanced lateral material relocation caused by projectile lateral expansion upon impact are the main factors responsible for promoting off-normal ejection. On the other hand, material ejection from randomly inclined surface areas and the influence of nearby topography are found to be responsible for enhancing ejection along the surface normal for rough surfaces. © 2016 American Vacuum Society.
[http://dx.doi.org/10.1116/1.4942202]

I. INTRODUCTION

Knowledge about the shape of angular distributions of particles ejected by projectile bombardment is important for both secondary ion mass spectrometry (SIMS) and especially for laser-based secondary neutral mass spectrometry (SNMS). In SIMS, a wide angular spread of sputtered particles may have a negative impact on the mass resolution. In SNMS, the effective overlap of the expanding plume with the laser irradiated volume is crucial for achieving high detection efficiency. While there is a plethora of experimental and theoretical studies of angular spectra stimulated by atomic projectiles,[1] much less is known about angular ejection caused by impacts of cluster projectiles. Yamada *et al.* have investigated experimentally directional ejection of particles from several inorganic samples bombarded with large Ar_n projectiles.[2–4] They have observed a strong off-normal ejection and attributed such behavior of the bombarded system to interaction of ejecting particles with projectile atoms. This effect is known as lateral sputtering. Similar behavior has been reported more recently for benzene sample bombarded with 15 keV Ar_{2953}.[5] Off-normal ejection also has been measured for intact benzopyrene molecules during C_{60} bombardment,[6] although the effect is not as pronounced as observed for large Ar clusters. Recent experiments of Chernysh *et al.* performed with Ar gas cluster projectiles on several polycrystalline metals and alloys,[7,8] in general, have confirmed observations of Yamada *et al.* However, a

different shape of angular distributions was observed when Mo and W surfaces were bombarded with 10 keV Ar_{800}. For these particular systems, angular spectra peak along the surface normal. This unusual behavior of angular emission was hypothesized to be due to a springlike ejection caused by a large elastic modulus of these materials.

So far, there are a very few theoretical studies of the effect of the cluster projectile size on the angular spectra.[4,9] Most computer studies have concentrated on probing the effect of the projectile size on the total sputtering yield,[10–14] or were limited to a selected projectile size when probing angular ejection.[4,15,16] The only systematic study of the effect of projectile size on the angular emission has been performed for small carbon projectiles.[9] So far, there are also a very few computer studies of morphology effect on the angular emission. The goal of the current study is to investigate the effect of the projectile size and the surface morphology on the angular spectra of atoms ejected from Ag(100) and Mo(100) samples. Argon gas cluster projectiles with sizes between 10 and 1000 are used to bombard these solids at normal incidence. A silver sample is selected to probe topography effects on angular emission using the roughened sample obtained in our previous study.[9] A molybdenum sample is chosen to probe hypothesis of springlike ejection mechanism proposed by Chernysh *et al.*[7,8]

II. MODELING

A detailed description of the molecular dynamics computer simulations used to model cluster bombardment can

---
a)Electronic mail: zbigniew.postawa@uj.edu.pl

be found elsewhere.[17] Briefly, the motion of particles is determined by integrating Hamilton's equations of motion. The forces among particles are described by a blend of pairwise additive and many-body potential energy functions. Embedded atom potentials (EAM) are used to describe the Ag–Ag (Ref. 18) and Mo–Mo (Ref. 19) interactions. These potentials were reparametrized to better describe system properties. The new parametrization has enabled, for instance, to eliminate overprediction of bonding in Ag dimers observed in the original Sandia EAM potential.[20] The interactions between Ar atoms in the projectile, and between the projectile atoms and all other particles in the system are described by the Lennard-Jones potential splined at small distances with the KrC potential to properly describe high-energy collisions.[21] The shape and size of the samples are chosen based on visual observations of collision cascades stimulated by impacts of 20 keV Ar_n projectiles. As a result, hemispherical samples with a radius of 15 nm are used. One hundred twenty one impacts are simulated to achieve statistically reliable data for Ag(100). At least two hundred impacts are sampled on Mo(100), because this material is more difficult to sputter due to its large binding energy. While samples with flat surfaces are created by the simulation program based on the structural properties of fcc Ag and bcc Mo solids, the samples used to model impacts at rough surfaces are cut-out from random locations of a silver master sample obtained in our previous work.[9] This master sample was created by a consecutive bombardment with 20 keV Ar_{872} at normal incidence up to a dose of $3 \times 10^{13}/cm^2$, which resulted in a surface with the RMS roughness of 2.7 nm. Ninety randomly selected impact points are chosen on this substrate, and hemispherical samples with a radius of 15 nm and a surface centered at these impact points are cut-out from the original block. Rigid and stochastic regions of 0.5 and 1.5 nm wide, respectively, are used to simulate the thermal bath that keeps the sample at required temperature, to prevent reflection of pressure waves from the boundaries of the system, and to maintain the shape of the sample.[17,22]

Ar_n cluster projectiles at normal incidence with n = 10–1000 are used to cover a wide range of experimentally interesting projectile sizes. The simulations are run at 0 K target temperature and extend up to 22 ps, which is long enough to achieve saturation in the sputtering yield versus time dependence. The calculations are performed with a LAMMPS code[23] that was modified for a more efficient modeling of sputtering phenomena.

III. RESULTS AND DISCUSSION

A. Effect of the projectile size

The total sputtering yields of atoms ejected from Ag(100) and Mo(100) surfaces by impacts of 10 keV Ar_n projectiles at normal incidence as a function of projectile size are shown in Fig. 1. The sputtering yields for projectiles between Ar_{20} and Ar_{250} are approximately 2.4 times larger for Ag(100) as compared to Mo(100). This value correlates very well with the inverse of the ratio of sublimation energies of these two
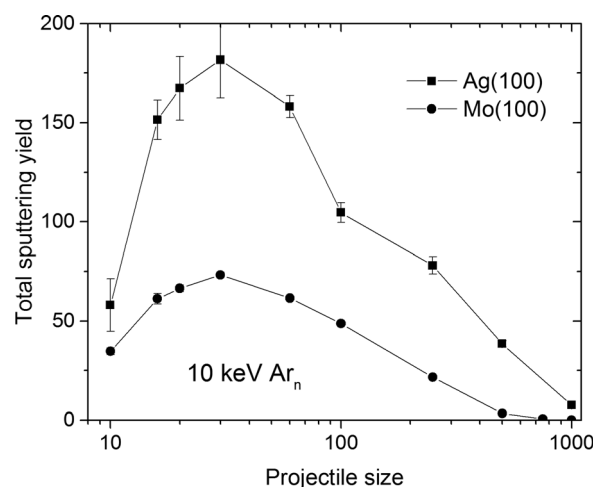

FIG. 1. Dependence of the total sputtering yield of Ag (square) and Mo (circle) atoms on the projectile size sputtered from Ag(100) and Mo(100) surfaces by 10 keV Ar_n gas cluster projectiles at normal incidence.

systems (2.9 eV for Ag and 6.8 eV for Mo).[24] The total sputtering yield strongly depends on the size of the projectile. The yield has a maximum near Ar_{30} for both silver and molybdenum. For larger clusters, the yield decreases faster for the Mo sample than for Ag, because of the larger binding energy of Mo. The presence of maximum in the sputtering yield versus projectile size dependence has already been observed in studies with smaller carbon clusters.[10,11] It has been attributed to an interplay between the density of deposited energy, energy deposition depth, and the binding energy of the solid.[10,11,25] The optimal cluster size was found to depend on the impact energy, shifting to larger clusters as the kinetic energy increases.[10]

Figure 2 presents polar and azimuthal distributions of the mass deposited at the hypothetical hemispherical collector centered in the middle of the surface. The distributions are calculated for 10 keV Ar_{60}, Ar_{250}, and Ar_{500} using a procedure characteristic to measurements performed with a mass collector. In the adopted approach, a single Ag_n particle deposits a mass corresponding to n silver atoms, rather than stimulates a single pulse in a mass spectrometer. Application of such a procedure is necessary in order to compare current results with the experimental angular spectra, which were measured with such a technique. Such an approach is also required because a flux of particles sputtered by cluster projectiles contains a significant contribution of Ag multimers. For a wide range of projectile sizes, Wehner spots[26] are visible at the collector. This observation is surprising because it is known that sputtering induced by cluster projectiles has a mesoscopic character.[17,27] The data shown in Fig. 2 indicate that regardless of a large material alteration caused by an impact of massive projectile, the bombarded system keeps memory about the geometry of the original surface structure. This memory becomes to fade away, however, when Ar_{500} projectiles are used. Inspection of the sputtering animations indicates that azimuthal randomization is not caused by surface amorphization, but by collisions of departing particles with Ar projectile atoms.
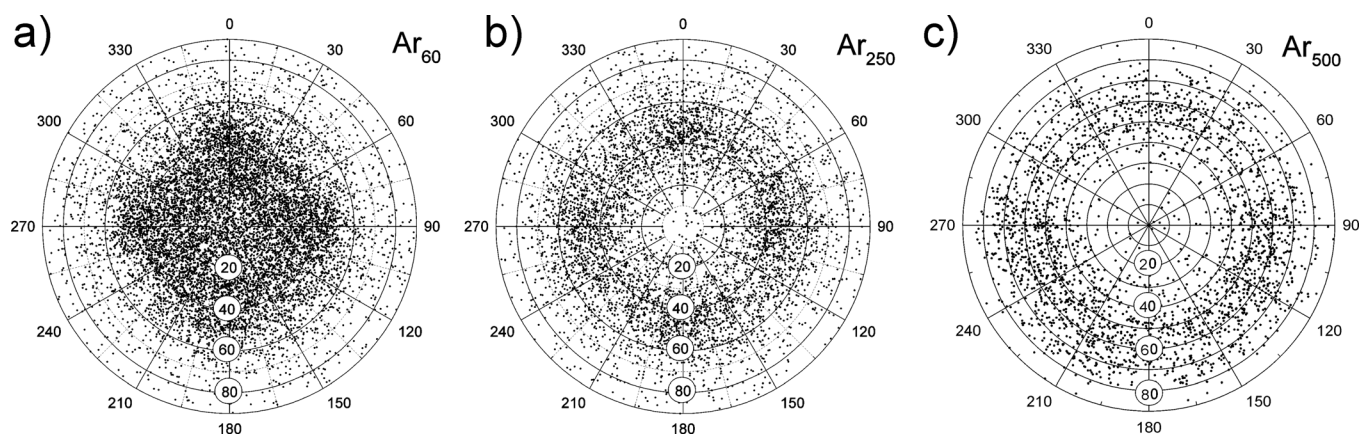
FIG. 2. Polar and azimuthal distribution of the mass deposited at the hypothetical hemispherical collector above the Ag(100) surface after bombardment with (a) 10 keV Ar_{60}, (b) 10 keV Ar_{250}, and (c) 10 keV Ar_{500} at normal incidence. Polar angles are indicated by number in circles while azimuthal angles are marked by numbers arranged around the plot.

The data shown in Fig. 2 indicate that the most efficient emission shifts to larger angles with the increase in the projectile size. However, just looking at a density of dots can be misleading as many dots correspond to deposition of dimers, trimers, and larger multimers. As the relative contribution of multimers increases with the size of the Ar cluster, the effect will be particularly visible for large projectiles. To take this effect into account and to obtain statistically reliable data, we plot azimuthally and energy-integrated peak normalized polar angle distributions of Ag and Mo atoms ejected from Ag(100) and Mo(100). The results are shown in Fig. 3. The distributions are rescaled to the same solid angle to eliminate a shift of the spectra to larger polar angles being caused by just collecting material from a larger area of the detector for a constant step in polar angle. For small projectiles, like Ar_{10}, angular distributions peak near the surface normal. The peak position shifts to larger polar angles as the projectile size increases. For large projectiles, like Ar_{500} or Ar_{1000}, most of atoms are ejected at very large polar angles, which agree with measurements performed by Yamada *et al.*[2,3] The low-angle ejection is influenced more than emission at large polar angles by changing the projectile size. For instance, a change from Ar_{10} into Ar_{100}, and then Ar_{500} leads to a signal decrease by factors of 2.1 and 366 for 0°, while the signal is

actually increased by factors of 2.2 and 1.7 for the 60° polar angle. The projectile kinetic energy influences the shape of angular spectra. The effect is more pronounced for smaller projectiles. For instance, the angular spectrum of Ag sputtered by 20 keV Ar_{60} has a maximum at 0° polar angle and a second peak near 25°. The azimuthal anisotropy is much less pronounced as compared to 10 keV impact, which agrees with our previous data for 20 keV C_{60} (Ref. 9) (not shown). On the other hand, the spectrum of Ag sputtered by 20 keV Ar_{1000} peaks near 58° with only slightly larger normal ejection (see below).

The data presented in Fig. 3 show that sputtering of Ag(100) and Mo(100) systems is qualitatively similar. For molybdenum, there is a small shift in peak positions to larger polar angles as compared to Ag. The main difference between sputtering of Ag and Mo is less efficient material ejection from molybdenum due to a much stronger bonding of this material as seen in Fig. 1. Unfortunately, because of a very low signal, angular emission of Mo atoms at conditions used in experiments of Chernysh *et al.*[7,8] could not be investigated. Even for 400 impacts of 10 keV Ar_{1000}, a total ejection of barely nine molybdenum atoms is observed thus no reliable conclusions can be drawn. Nevertheless, it is observed that all these particles are emitted at large off-normal angles.
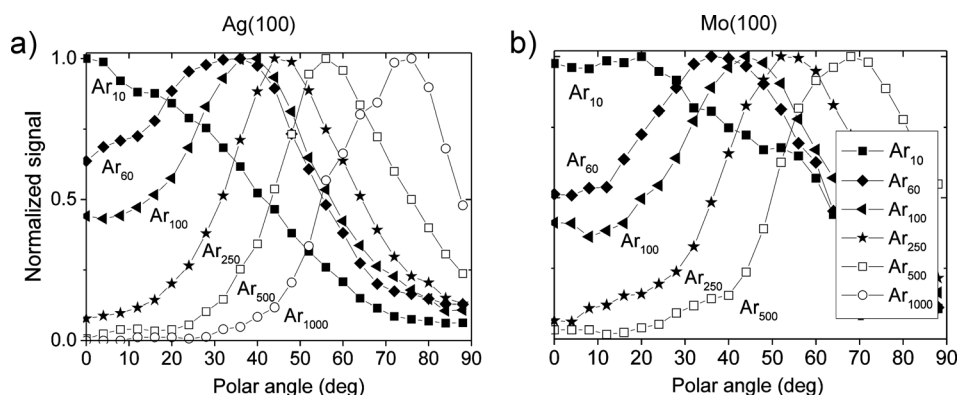

FIG. 3. Peak normalized azimuthally and energy-integrated polar angle distributions of particles sputtered by the 10 keV Ar_n projectiles at normal incidence from (a) Ag(100) and (b) Mo(100) flat surfaces. All ejected particles are used to create these plots to mimic distributions obtained with a mass collector technique.
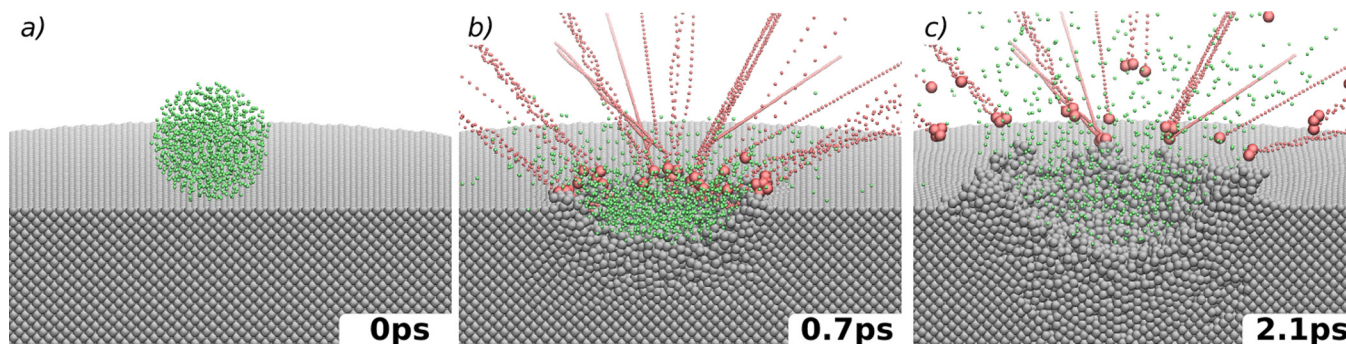
FIG. 4. (Color online) Temporal evolution of Ag(100) system bombarded by 10 keV Ar_{1000} at normal incidence. Silver atoms are represented by gray spheres. Small (green) spheres and lines of spheres represent Ar and sputtered Ag atoms, respectively. Lines of spheres represent trajectories of silver atoms being ejected.

The studies performed with kilo-electron-volt medium cluster projectiles like C_{60} have shown that material ejection is caused mainly by two processes.[6,27] Impact of kilo-electron-volt cluster projectiles leads to formation of an energized zone that expands radially leading to formation of the crater.[5,6,28] During this process, atoms are moved toward the surface by a mechanism that resembles a fluid-flow along the walls of the forming crater.[25] This process leads to emission of energetic particles from the corona of the forming crater, predominantly at off-normal directions.[5,6] At later-times, particles begin to effuse with low kinetic energy from inside the crater. For some time, this process dominates total ejection before the emission finally disappears. The angular distribution of effusing particles is more uniform.[6] It is emission of these particles that contributes mostly to the ejected plume in directions close to the surface normal.

The sputtering process induced by medium and large clusters has many similarities. However, they also have important differences. The first difference between these projectiles is a much larger momentum of the large gas cluster projectiles, which leads to a larger penetration depth, especially in soft materials.[29] A second difference is a larger lateral component of the force exerted on the surrounding media by large Ar projectiles during their initial compression/decompression phase. This lateral expansion is a result of interaction between the incoming and backreflected projectile atoms, which leads to a formation of strong side jetting of Ar atoms.[27,30,31] The effect increases with the size of the projectile. One consequence of this process is a faster increase in the crater diameter as compared to a change of its depth. But the most important consequence of side jetting is a transfer of lateral momentum to the surrounding media leading to off-normal emission of atoms from the crater corona.[27] It should be pointed out, however, that larger momentum will not necessarily lead to larger sputtering. Instead, it will usually cause a more extensive ion-induced mixing.[27,32] The third difference between medium and large cluster impacts is formation of the hovering cloud when clusters composed from hundreds or thousands of atoms are used, as shown in Fig. 4. Inspection of this figure indicates that formation of the cloud has a minor impact on the ejection of atoms from the rim of the forming crater, as the cloud is mostly confined inside the volume of the crater.

Furthermore, atoms ejecting from the rim have relatively high kinetic energies, which make them less prone to any influence. On the other hand, the effusion process can be blocked by a cloud of slow projectile atoms that require many picoseconds to disperse. After a long time, most of the primary kinetic energy is already carried away from the impact volume, and only few atoms have sufficient kinetic energy to depart from the surface. Consequently, the Ar cloud will predominantly reduce intensity of near normal ejection, causing the peak in angular spectra to shift to larger polar angles. Both these effects are indeed visible in Fig. 3. The magnitude of the influence of cloud blocking increases with the size of the projectile as more atoms are available to form the cloud. In addition, these atoms will also remain for a longer time above the bombarded area because the projectile becomes slower if its total kinetic energy is kept constant. Argon cloud is not formed during impacts of small and medium-size clusters. These projectiles do not contain sufficient number of atoms. Moreover, their initial velocities are also high, which results in a fast dispersion of the cloud.

B. Effect of the surface morphology

Simulations performed with Au_3 and C_{60} projectiles have shown that the surface morphology can also have an influence on the polar angle distributions of emitted atoms.[9] The angular spectra obtained from flat and rough Ag surfaces
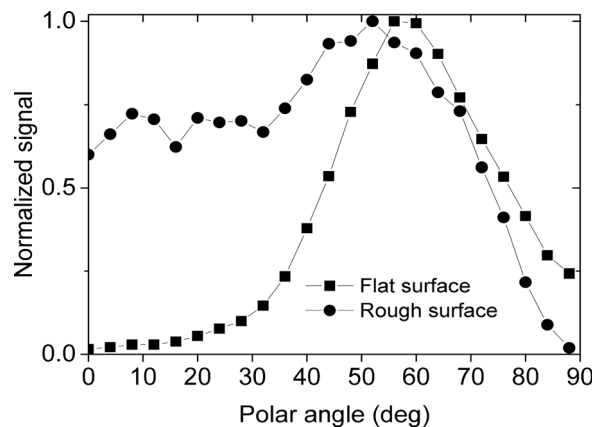

FIG. 5. Peak normalized polar angle distributions of Ag atoms sputtered by 20 keV Ar_{1000} at normal incidence from flat and roughened Ag surface. The roughened surface has the RMS roughness of 2.7 nm.

bombarded by 20 keV Ar_{1000} at normal incidence are shown in Fig. 5. The kinetic energy of the Ar projectile is higher than used so far to maintain consistency with conditions used to create roughened master sample.[9] It is evident that the angular spectrum calculated at a corrugated sample exhibits a more pronounced ejection in directions near the surface normal. To understand this change, three impact scenarios are selected to represent sufficiently wide range of possible sputtering events. They correspond to the bombardment of the top of the mound, the bottom of the valley, and finally, the side of the mound, as shown in Fig. 6. The details of material relocation inside the sample bombarded by a continuous flux of cluster projectiles have been already investigated.[27,32,33] In this work, we focus on directional aspects of sputtering. The trajectories of ejected atoms are marked by red lines in Fig. 6. Regardless of differences in the bombarded environment, there are several observations that are universal for all these scenarios. First, although most of the ejecting atoms are originally located in the area below the projectile, their final point of separating from the surface may occur quite distant from the original point of impact.

This is clearly visible in Figs. 6(a) and 6(c). Usually, these atoms collide with nearby topographical structures and are emitted closer to the surface normal. Because atoms are ejected from areas distant from the impact point, movement
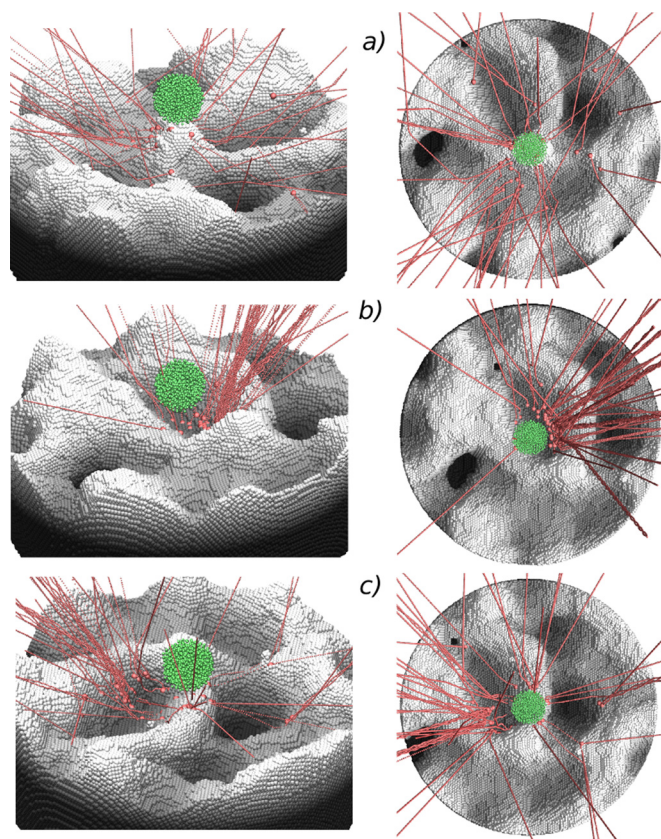
of these atoms is less influenced by collisions with projectile atoms forming a cloud. Secondly, trajectories of ejecting atoms are usually deflected in directions closer to the 0° polar angle by a local morphology. The most efficient deflection occurs when bombarding the bottom of the valley, as shown in Fig. 6(b). However, similar process also occurs when a side of the mound is hit, where atoms are originally ejected downwards. Most of these atoms fill the valleys. However, some of them are backreflected and finally ejected. Their trajectories are influenced in a similar way to the atoms sputtering from the bottom of the valley. Finally, most of oblique ejections occur when a top of the mound is hit, as shown in Fig. 6(a). But also in this case, the nearby morphology can deflect some of these trajectories toward the sample normal. The overall effect of all these scenarios is redirection of the ejecting flux to lower polar angles, which is indeed seen in Fig. 5. Similar scenarios do not occur at flat surfaces.

IV. SUMMARY AND CONCLUSIONS

Angular distributions of particles sputtered by argon gas cluster projectiles have been investigated. It has been shown that both projectile size and surface morphology have a significant influence on the angular spectra. For clusters composed of less than 30 atoms, angular distributions are peaked near the direction normal to the surface. From the point of view of both SIMS and SNMS, such behavior of the ejecting plume is optimal as the angular spread is low (SIMS) and it is relatively simple to overlap the ionizing laser with the ejecting plume (SNMS). The peak in the angular distributions shifts toward off-normal direction for larger projectiles, and sputtering is dominated by off-normal emission for clusters composed of few hundred Ar atoms. From the point of view of both SIMS and SNMS, this is a less optimal scenario, especially, if a resonant photoionization is used to create ions in SNMS. In this case, it will be more difficult to simultaneously ionize atoms moving toward and along directions of the incoming laser beam due to a Doppler effect.

Surface morphology of a roughened surface versus a flat surface enhances emission closer to the surface normal in the angular spectra. Such behavior seen in angular distributions occurs because many atoms are ejected from corrugated surfaces from areas that are not located directly below the impacting cluster. This feature reduces the effect of the hovering cloud and promotes redirection of trajectories toward the surface normal by collisions with walls of nearby topographical structures.

The phenomenon reported in experiments of Chernysh *et al.*[7,8] could not be reproduced in our study. As a result, it is not possible to verify ejection model proposed in these papers. It should be pointed out, however, that experiments with Mo and W were performed under conditions where the sputtering yield is very low. For example, the yield calculated for 10 keV Ar_{750} bombarding Mo(100) is less than 0.5 atoms per cluster projectile which is almost 2 orders of magnitude smaller than the most efficient ejection induced by impact of 10 keV Ar_{30}. Gas cluster ion beams used in experiments

FIG. 6. (Color online) Trajectories of atoms ejected from corrugated surface of Ag bombarded by 20 keV Ar_{1000} at normal incidence at (a) top of the mound, (b) at the bottom of the valley and (c) at the side of the mound. Trajectories of ejecting atoms are depicted by lines of spheres. Nonejected Ag atoms are marked by gray spheres. They are shown in their original positions. Spheres above the surface indicate initial position of Ar atoms.

contain projectiles with a distribution of sizes. The ion source used in the system where the Mo measurements were performed has a peak in the size distribution at 800 Ar atoms[7,8] with a full width at half maximum of around 1000 atoms.[34] It is, therefore, possible that the measured sputtering is caused by smaller clusters, which lead to a more efficient ejection in directions closer to the surface normal.

ACKNOWLEDGMENTS

[1] W. O. Hofer, Top. Appl. Phys. **64**, 15 (1991); and references therein.

[2] I. Yamada, J. Matsuo, N. Toyoda, and A. Kirkpatrick, Mater. Sci. Eng., R **34**, 231 (2001).

[3] N. Toyoda, H. Kitani, N. Hagiwara, T. Aoki, J. Matsuo, and I. Yamada, Mater. Chem. Phys. **54**, 262 (1998).

[4] Z. Insepov and I. Yamada, Nucl. Instrum. Methods B **99**, 248 (1995).

[5] B. Czerwinski, L. Rzeznik, R. Paruch, B. J. Garrison, and Z. Postawa, Nucl. Instrum. Methods B **269**, 1578 (2011).

[6] D. A. Brenes, Z. Postawa, A. Wucher, P. Blenkinsopp, B. J. Garrison, and N. Winograd, J. Phys. Chem. Lett. **2**, 2009 (2011).

[7] V. S. Chernysh, A. E. Ieshkin, and Y. A. Ermakov, Appl. Surf. Sci. **326**, 285 (2015).

[8] A. E. Ieshkin, Y. A. Ermakov, and V. S. Chernysh, Nucl. Instrum. Methods B **354**, 226 (2015).

[9] R. Paruch, L. Rzeznik, M. F. Russo, B. J. Garrison, and Z. Postawa, J. Phys. Chem. C **114**, 5532 (2010).

[10] B. Czerwinski, L. Rzeznik, K. Stachura, R. Paruch, B. J. Garrison, and Z. Postawa, Vacuum **82**, 1120 (2008).

[11] K. E. Ryan and B. J. Garrison, Anal. Chem. **80**, 6666 (2008).

[12] T. Aoki, T. Seki, J. Matsuo, Z. Insepov, and I. Yamada, Nucl. Instrum. Methods B **153**, 264 (1999).

[13] C. Anders, H. M. Urbassek, and R. E. Johnson, Phys. Rev. B **70**, 155404 (2004).

[14] J. Matsuo, S. Ninomiya, Y. Nakata, K. Ichiki, T. Aoki, and T. Seki, Nucl. Instrum. Methods B **257**, 627 (2007).

[15] J. Samela and K. Nordlund, Nucl. Instrum. Methods B **263**, 375 (2007).

[16] S. Bouneau, S. Della Negra, D. Jacquet, Y. Le Beyec, M. Pautrat, M. H. Shapiro, and T. A. Tombrello, Phys. Rev. B **71**, 174110 (2005).

[17] B. J. Garrison and Z. Postawa, Mass Spectrom. Rev. **27**, 289 (2008).

[18] P. L. Williams, Y. Mishin, and J. C. Hamilton, Model. Simul. Mater. Sci. **14**, 817 (2006).

[19] G. J. Ackland and R. Thetford, Philos. Mag. A **56**, 15 (1987).

[20] S. M. Foiles, M. I. Baskes, and M. S. Daw, Phys. Rev. B **33**, 7983 (1986).

[21] R. A. Aziz and M. J. Slaman, Mol. Phys. **58**, 679 (1986).

[22] Z. Postawa, B. Czerwinski, M. Szewczyk, E. J. Smiley, N. Winograd, and B. J. Garrison, Anal. Chem. **75** 4402 (2003).

[23] S. J. Plimpton, J. Comput. Phys. **117**, 1 (1995).

[24] P. Sigmund, Phys. Rev. **184**, 383 (1969).

[25] M. F. Russo and B. J. Garrison, Anal. Chem. **78**, 7206 (2006).

[26] G. K. Wehner, J. Appl. Phys. **26**, 1056 (1955).

[27] R. J. Paruch, Z. Postawa, and B. J. Garrison, Acc. Chem. Res. **48**, 2529 (2015).

[28] A. Delcorte, B. J. Garrison, and K. Hamraoui, Anal. Chem. **81**, 6676 (2009).

[29] V. N. Popok, J. Samela, K. Nordlund, and E. E. B. Campbell, Phys. Rev. B **82**, 201403 (2010).

[30] L. Rzeznik, B. Czerwinski, B. J. Garrison, N. Winograd, and Z. Postawa, J. Phys. Chem. C **112**, 521 (2008).

[31] H. M. Urbassek and S. N. Sun, *Nanodroplets* (Springer, New York/Heidelberg/Dordrecht/London, 2013), p. 169.

[32] R. J. Paruch, B. J. Garrison, and Z. Postawa, Anal. Chem. **84**, 3010 (2012).

[33] M. F. Russo, Z. Postawa, and B. J. Garrison, J. Phys. Chem. C **113**, 3270 (2009).

[34] A. A. Andreev, V. S. Chernysh, Y. A. Ermakov, and A. E. Ieshkin, Vacuum **91**, 47 (2013).